Porous silicon integrated Mach-Zehnder interferometer waveguide for biological and chemical sensing

Kyowon Kim* **and Thomas E. Murphy**

Institute for Research in Electronics and Applied Physics, University of Maryland, College Park, MD 20742, USA

*kyowon@umd.edu

Abstract: Optical waveguides comprised of nanoporous materials are uniquely suited for on-chip sensing applications, because they allow for a target chemical or analyte to directly infiltrate the optical material that comprises the core of the waveguide. We describe here the fabrication and characterization of nanoporous waveguides, and demonstrate their usefulness in measuring small changes in refractive index when exposed to a test analyte. We use a process of electrochemical etching and laser oxidation to produce channel waveguides and integrated on-chip Mach-Zehnder structures, and we compare the responsivity and interferometric stability of the integrated sensor to that of a fiber-based interferometer. We quantify the detection capability by selectively applying isopropanol to a 200 μm length waveguide segment in one arm of the interferometer, which produces a phase shift of 9.7π. The integrated interferometer is shown to provide a more stable response in comparison to a comparable fiber-based implementation.

OCIS codes: (130.6010) Sensors; (060.2370) Fiber optics sensors; (130.3120) Integrated optics devices; (280.4788) Optical sensing and sensors; (230.7370) Waveguides; (160.4236) Nanomaterials.

References and links

1. J. B. Jensen, L. H. Pedersen, P. E. Hoiby, L. B. Nielsen, T. P. Hansen, J. R. Folkenberg, J. Riishede, D. Noordegraaf, K. Nielsen, A. Carlsen, and A. Bjarklev, "Photonic crystal fiber based evanescent-wave sensor for detection ofbiomolecules in aqueous solutions," Opt. Lett. **29**, 1974–1976 (2004).
2. C. A. Rowe-Taitt, J. W. Hazzard, K. E. Hoffman, J. J. Cras, J. P. Golden, and F. S. Ligler, "Simultaneous detection of six biohazardous agents using a planar waveguide array biosensor," Biosens. Bioelectron. **15**, 579–589 (2000).
3. M.-L. Anne, J. Keirsse, V. Nazabal, K. Hyodo, S. Inoue, C. Boussard-Pledel, H. Lhermite, J. Charrier, K. Yanakata, O. Loreal, J. Le Person, F. Colas, C. Compère, and B. Bureau, "Chalcogenide glass optical waveguides for infrared biosensing," Sensors **9**, 7398–7411 (2009).
4. P. Polynkin, A. Polynkin, N. Peyghambarian, and M. Mansuripur, "Evanescent field-based optical fiber sensing device for measuring the refractive index of liquids in microfluidic channels," Opt. Lett. **30**, 1273–1275 (2005).
5. S. Campopiano, R. Bernini, L. Zeni, and P. M. Sarro, "Microfluidic sensor based on integrated optical hollow waveguides," Opt. Lett. **29**, 1894–1896 (2004).
6. V. J. Cadarso, C. Fernández-Sánchez, A. Llobera, M. Darder, and C. Domínguez, "Optical biosensor based on hollow integrated waveguides," Anal. Chem. **80**, 3498–3501 (2008).
7. J. Gao, T. Gao, Y. Y. Li, and M. J. Sailor, "Vapor sensors based on optical interferometry from oxidized microporous silicon films," Langmuir **18**, 2229–2233 (2002).
8. L. D. Stefano, L. Rotiroti, I. Rea, L. Moretti, G. D. Francia, E. Massera, A. Lamberti, P. Arcari, C. Sanges, and I. Rendina, "Porous silicon-based optical biochips," J. Opt. A: Pure Appl. Opt. **8**, S540 (2006).

#191714 - $15.00 USD Received 4 Jun 2013; revised 19 Jul 2013; accepted 2 Aug 2013; published 12 Aug 2013

9. P. A. Snow, E. K. Squire, P. S. J. Russell, and L. T. Canham, "Vapor sensing using the optical properties of porous silicon bragg mirrors," J. Appl. Phys. **86**, 1781–1784 (1999).
10. M. A. Anderson, A. Tinsley-Bown, P. Allcock, E. A. Perkins, P. Snow, M. Hollings, R. G. Smith, C. Reeves, D. J. Squirrell, S. Nicklin, and T. I. Cox, "Sensitivity of the optical properties of porous silicon layers to the refractive index of liquid in the pores," Phys. Status Solidi A **197**, 528–533 (2003).
11. S. Chan, P. Fauchet, Y. Li, L. Rothberg, and B. Miller, "Porous silicon microcavities for biosensing applications," Phys. Status Solidi A **182**, 541–546 (2000).
12. L. D. Stefano, I. Rendina, L. Moretti, and A. M. Rossi, "Optical sensing of flammable substances using porous silicon microcavities," Mater. Sci. Eng. B **100**, 271–274 (2003).
13. L. D. Stefano, L. Moretti, A. Lamberti, O. Longo, M. Rocchia, A. M. Rossi, P. Arcari, and I. Rendina, "Optical sensors for vapors, liquids, and biological molecules based on porous silicon technology," IEEE Trans. Nanotechnol. **3**, 49–54 (2004).
14. L. A. DeLouise, P. M. Kou, and B. L. Miller, "Cross-correlation of optical microcavity biosensor response with immobilized enzyme activity. insights into biosensor sensitivity," Anal. Chem. **77**, 3222–3230 (2005).
15. H. Zhang, Z. Jia, X. Lv, J. Zhou, L. Chen, R. Liu, and J. Ma, "Porous silicon optical microcavity biosensor on silicon-on-insulator wafer for sensitive DNA detection ," Biosens. Bioelectron. **44**, 89–94 (2013).
16. R. Liu, T. A. Schmedake, Y. Y. Li, M. J. Sailor, and Y. Fainman, "Novel porous silicon vapor sensor based on polarization interferometry," Sens. Actuators B **87**, 58–62 (2002).
17. J. Álvarez, P. Bettotti, I. Suárez, N. Kumar, D. Hill, V. Chirvony, L. Pavesi, and J. Martínez-Pastor, "Birefringent porous silicon membranes for optical sensing," Opt. Express **19**, 26106–26116 (2011).
18. E. De Tommasi, L. D. Stefano, I. Rea, V. Di Sarno, L. Rotiroti, P. Arcari, A. Lamberti, C. Sanges, and I. Rendina, "Porous silicon based resonant mirrors for biochemical sensing," Sensors **8**, 6549–6556 (2008).
19. I. Rea, M. Iodice, G. Coppola, I. Rendina, A. Marino, and L. D. Stefano, "A porous silicon-based bragg grating waveguide sensor for chemical monitoring," Sens. Actuators B **139**, 39–43 (2009).
20. G. Rong, "Highly sensitive porous silicon membrane waveguide sensor using ultra-high order mode," in "Symp. Photonics Optoelectron.", (2009), pp. 1–4.
21. Y. Jiao and S. M. Weiss, "Design parameters and sensitivity analysis of polymer-cladded porous silicon waveguides for small molecule detection," Biosens. Bioelectron. **25**, 1535–1538 (2010).
22. X. Wei and S. M. Weiss, "Guided mode biosensor based on grating coupled porous silicon waveguide," Opt. Express **19**, 11330–11339 (2011).
23. A. Loni, L. T. Canham, M. G. Berger, R. Arens-Fischer, H. Munder, H. Luth, H. F. Arrand, and T. M. Benson, "Porous silicon multilayer optical waveguides," Thin Solid Films **276**, 143–146 (1996).
24. J. Charrier, C. Lupi, L. Haji, and C. Boisrobert, "Optical study of porous silicon buried waveguides fabricated from p-type silicon," Mater. Sci. Semicond. Process. **3**, 357–361 (2000).
25. P. Pirasteh, J. Charrier, Y. Dumeige, P. Joubert, S. Haesaert, and L. Haji, "Further results on porous silicon optical waveguides at 1.55 μm," Phys. Status Solidi A **204**, 1346–1350 (2007).
26. M. Hiraoui, M. Guendouz, N. Lorrain, L. Haji, and M. Oueslati, "Buried anti resonant reflecting optical waveguide based on porous silicon material for an integrated Mach Zehnder structure," Appl. Phys. Lett. **101**, 191114 (2012).
27. A. M. Rossi, G. Amato, V. Camarchia, L. Boarino, and S. Borini, "High-quality porous-silicon buried waveguides," Appl. Phys. Lett. **78**, 3003–3005 (2001).
28. J. Xia, A. M. Rossi, and T. E. Murphy, "Laser-written nanoporous silicon ridge waveguide for highly sensitive optical sensors," Opt. Lett. **37**, 256–258 (2012).
29. G. Rong, J. D. Ryckman, R. L. Mernaugh, and S. M. Weiss, "Label-free porous silicon membrane waveguide for dna sensing," Appl. Phys. Lett. **93**, 161109 (2008).

1. Introduction

Optical sensors are attracting attention for a variety of applications including medical diagnostics, environmental monitoring, security and manufacturing. The ability to remotely probe, sense, diagnose or measure a target analyte through optical means is particularly important in applications that are otherwise not amenable to or accessible by electrical means. Waveguide-based optical sensing systems are more appealing than those based on bulk measurements because they offer the possibility for miniaturization, integration and parallelization.

Many optical waveguide sensors rely on a small refractive index change that occurs when a target analyte binds to or otherwise interacts with an optical surface. One of the most studied refractive index sensor designs is the solid core evanescent wave sensor, which relies on the small overlap between the evanescent tail of an optical mode with a surface-bound analyte [1–4] – typically a weak effect that requires a long interaction length to produce a measurable signal.

#191714 - $15.00 USD Received 4 Jun 2013; revised 19 Jul 2013; accepted 2 Aug 2013; published 12 Aug 2013

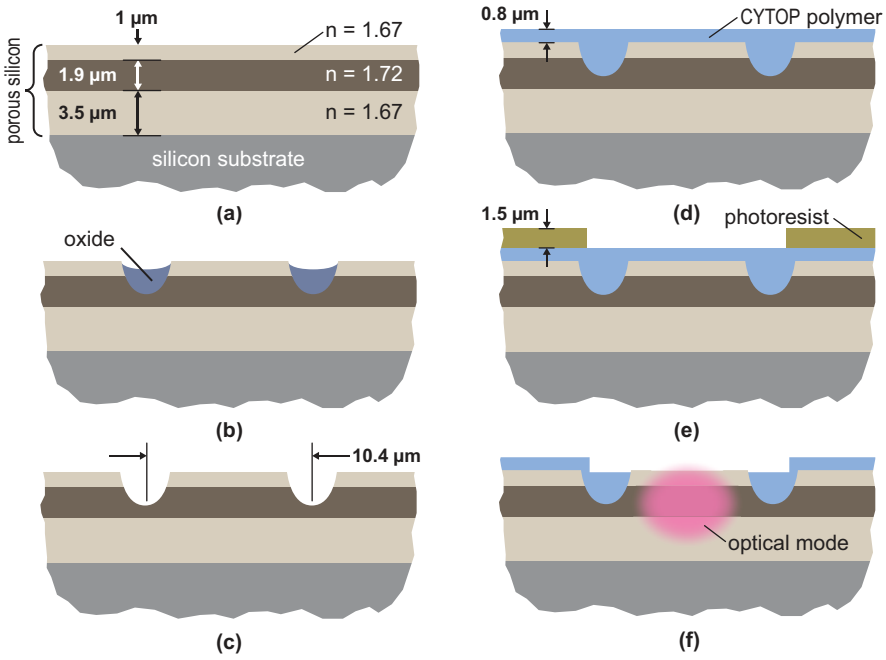

Fig. 1. Fabrication process used to produce integrated porous silicon waveguides. (a) A three-layer planar waveguide is formed by electrochemical etching of crystalline silicon. (b) Two parallel lines are inscribed using direct-write laser oxidation, to form the left and right boundaries of the optical waveguide. (c) The oxidized regions are removed in a solution of dilute HF. (d) A planarizing polymer layer (CYTOP) is spin-coated over the structure. (e) The sensing window is photolithographically defined, and (f) reactive ion etching is used to expose the underlying porous silicon waveguide.

Moreover, exposing the evanescent tail of the mode can make an optical waveguide susceptible to macroscopic particles and other unwanted contaminants (in addition to the analyte) that impair the function of the sensor. More recently, microfluidic waveguide sensors have been introduced to overcome limitations of evanescent wave sensors [5, 6], however the need for microfluidic circulation can complicate the device operation and poses a challenge for miniaturization.

Nanoporous silicon offers a unique solution to the above-mentioned challenges, by providing a material with large surface area to volume ratio that is ideal for capturing and concentrating a target analyte into a small volume. Provided the pore feature size is smaller than the optical wavelength, the resulting material behaves as an effective dielectric with optical properties that depend on the infiltrating substance. In comparison to evanescent sensors, the proposed device allows far greater overlap between the optical mode and the material to be sensed, thus enabling sensitive detection in a compact device, with a small analyte volume. The nanoscale porous structure prohibits fouling of the detector by larger particles. As we demonstrate here, the on-chip integration in a Mach-Zehnder interferometer (MZI) structure permits interferometric measurement while avoiding the problems of phase instability that plague free-space or fiber-based interferometers.

Several porous silicon sensor designs have been proposed and demonstrated. Many prior devices rely on observation of the reflection interference spectrum from porous structures, including single layers [7, 8], Bragg mirrors [9, 10] or resonant cavities [11–15]. Transmission

#191714 - $15.00 USD Received 4 Jun 2013; revised 19 Jul 2013; accepted 2 Aug 2013; published 12 Aug 2013

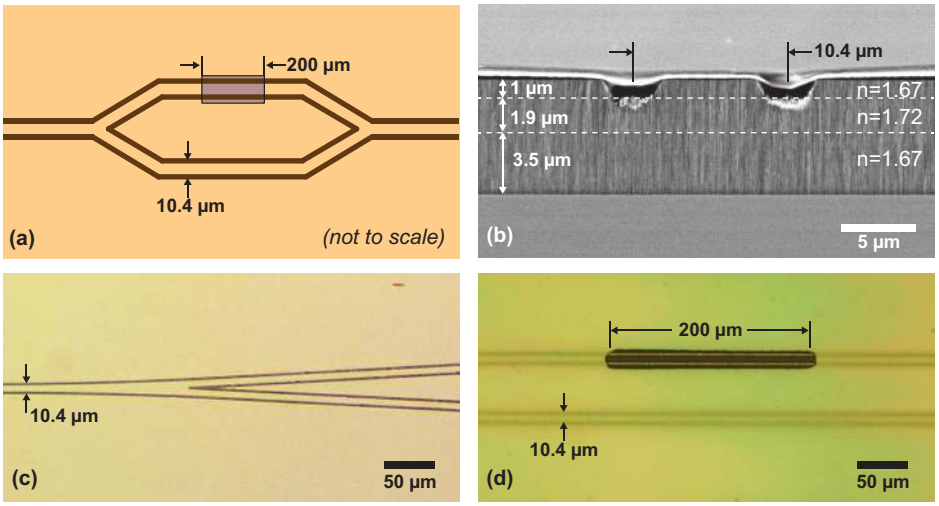

Fig. 2. (a) Schematic of integrated MZI waveguide. (b) Cross-sectional scanning electron micrograph (SEM) of a single waveguide. (c) Optical micrograph of Y-branch. (d) Optical micrograph showing selectively exposed sensing window in one arm of the interferometer.

measurements have also been achieved by measuring the change in birefringence when a free-standing porous substrate is filled with a solvent or analyte [16, 17]. All of these devices that utilize an optical path that is perpendicular to porous silicon substrate, and therefore inherently suffer from limited sensitivity because of the short interaction length. Further, many of them require a relatively wide-range tunable laser or broadband light source to detect shifts in the spectral pattern.

A solution to this issue is to employ a waveguide structure that confines light in two dimensions and guides parallel to substrate. This design allows relatively long interaction length by simply extending the length of sensing area. Vertical confinement of light in porous silicon can be easily achieved by controlling etching current, thus introducing high index guiding layer in between lower index cladding layers. Several recent studies used this multi layer core and cladding structure as a planar waveguide with coupling structures to increase sensitivity [18–22]. However waveguides that confine light in two dimensions require some transverse confinement structure in addition to a planar dielectric stack. Techniques to incorporate transverse confinement include lithographic patterning and dry etching of multi layers [23], masking of the crystalline silicon substrate prior to electrochemical etching [24–26], direct laser oxidation of the surrounding regions, as we use here [27, 28].

Here we describe the fabrication and characterization of a single-mode porous silicon integrated MZI waveguide, with a polymer passivation layer used to confine the analyte to a prescribed region. The device is fabricated using direct-write laser oxidation of a planar porous multilayer substrate, to produce a fully-confined optical waveguide. The functionality of the sensor is demonstrated using isopropyl alcohol as a test analyte, which is shown to produce a large, measurable phase shift, even when the exposed region is confined to be only 200 μm. We compare the performance of the integrated MZI to a comparable fiber-based MZI, and show greatly improved stability.

#191714 - $15.00 USD Received 4 Jun 2013; revised 19 Jul 2013; accepted 2 Aug 2013; published 12 Aug 2013

2. Fabrication and characterization

Figure 1 illustrates the process used to fabricate the waveguide sensors reported here. The porous waveguide was fabricated by electrochemical etching of a p-doped (1-5 mΩ cm) ⟨100⟩ crystalline silicon substrate in a 25% hydrofluoric acid solution (hydrofluoric acid, water, ethanol 1:1:2 by volume). A three-layer buried-core slab waveguide was formed by applying current density of 98.4 mA/cm^2 for the core layer and 121.5 mA/cm^2 for top and bottom cladding layers, thereby introducing a 1.9 μm-thick intermediate core layer with refractive index of 1.72 between 1.0 μm top and 3.5 μm bottom cladding layers with refractive index of 1.67. The layer profile was chosen to minimize loss and ensure single mode operation in vertical direction. The etch rate was 60.4 nm/sec and 69.6 nm/sec for the core and cladding, respectively, and the etching durations were adjusted to achieve the desired thickness.

The etch rates and refractive indices were calibrated by performing optical reflectance and profilometry measurements on separately-fabricated single-layer samples. The reflectance spectrum from a single porous layer on the (reflective) silicon substrate was measured using a tunable 1.55 μm laser, and the etch depth was then measured by profilometry, after selectively removing the porous layer in a solution of sodium hydroxide (NaOH.) The refractive indices were then calculated from the period of the fringes observed in reflectance.

The resulting slab waveguide was placed on a programmable XY translation stage, and a 532 nm continuous-wave (CW) laser with power of 25 mW was focused onto the surface through a 40×, 0.66 NA microscope objective, while the substrate was scanned at a speed of 0.4 mm/s. The 532 nm illumination is strongly absorbed in the porous layer, which produces a localized region of oxidized porous silicon, which was later selectively removed using a dilute solution of hydrofluoric acid. The resulting structure was partially oxidized in a rapid thermal annealing (RTA) furnace at 400°C for 5 min. in order to passivate the silicon surface. Figure 2(b) shows the cross-sectional micrograph of a completed single-mode optical waveguide formed by inscribing two such parallel lines.

Following fabrication of the waveguides, a low-index, 0.8 μm-thick planarizing polymer layer (CYTOP, Asahi Glass Co.) was spin-coated onto the waveguide and cured, followed by a 1.5 μm-thick photoresist imaging layer. Immediately prior to spin-coating the photoresist, the CYTOP layer was briefly exposed for 15 seconds in an oxygen plasma etcher, followed by application of hexamethyldisilazane (HMDS). Both steps were found to be effective in ensuring adequate adhesion of the photoresist layer. The photoresist was patterned using the same scanning laser lithography system described above, with a 10×, 0.25 NA microscope objective and 437 nm, 0.5 mW laser to selectively expose a 200 μm long region above the sensing arm of the interferometer. Following development, the underlying polymer was removed through reactive ion etching in an oxygen plasma, revealing the porous waveguide underneath. After lithographic processing, the device was cleaved to allow edge-coupling at the input and output facets. Figure 2(c)-(d) presents top-down optical micrographs of the Y-branch waveguide and the 200 μm exposed sensor region.

In order to ensure a stable and equal power splitting ratio for the Y-branches that comprise the MZI, it is essential that waveguides support only a single optical mode. In order to confirm that the waveguide is singlemode, we used an infrared camera to monitor both the power and mode shape emerging from the output of a simple Y-branch waveguide. A 1550 nm laser was coupled into single-branch facet through a lensed fiber and the emerging beams from the double-branch facet was focused on a phosphor-coated CCD camera through a 20× objective. The relative brightness between the two waveguides was observed at the output facet while moving the lensed fiber position on input facet. When the waveguide width was smaller than 10.4 μm, the light was equally split between the two output waveguides, as shown in Fig. 3(a), even when the position of the input lensed fiber was adjusted (Media 1), indicating that the waveguide

#191714 - $15.00 USD Received 4 Jun 2013; revised 19 Jul 2013; accepted 2 Aug 2013; published 12 Aug 2013

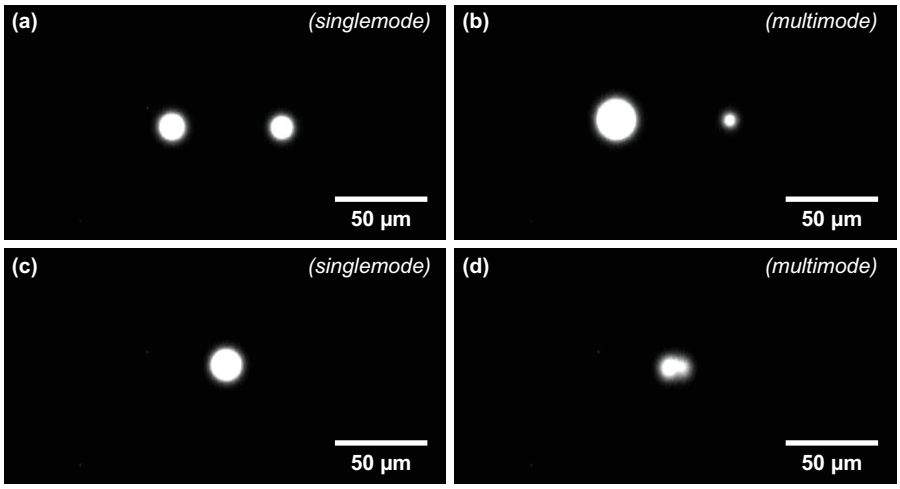

Fig. 3. Observations of optical pattern emerging from porous silicon waveguide for (a) singlemode waveguide with y-branch, (b) multimode optical waveguide with y-branch, (c) singlemode straight waveguide and (d) multimode straight waveguide. The corresponding multimedia files (Media 1, Media 2, Media 3 and Media 4) show that when the input fiber is moved, the output light distribution changes in the multimode case, but remains unchanged (apart from brightness) in the singlemode case.

is singlemode under these conditions. Conversely, for waveguides wider than 10.4 μm, the splitting ratio was observed to depend on the input coupling conditions indicating multimode behavior (Fig. 3(b), Media 2). Further measurements conducted on straight waveguides show that the output mode shape is independent of fiber position for the single-mode case (Fig. 3(c), Media 3), but depends strongly on the fiber position in the multimode case (Fig. 3(d), Media 4).

The waveguide propagation loss was estimated by performing cutback measurements of the transmission for straight waveguides of three different lengths. The input and output coupling losses were estimated by extrapolating the total insertion loss measurements to a device length of zero, and the excess scattering loss in the y-branch was calculated by comparing the total output power to that of a straight waveguide with the same length. The total waveguide insertion loss in a 12 mm long device was estimated to be 23 dB, including coupling loss (2 dB/facet), propagation loss (14 dB), and scattering loss in the y-branch (5 dB).

3. Experimental results

A fiber coupled 1550 nm continuous-wave laser with maximum power of 4 mW was coupled into input facet of MZI waveguide through a lensed fiber. The light emerging from the waveguide was collected with a second lensed fiber and photodiode, which records the interferometric signal, as illustrated in Fig. 4(a).

For comparison, we conducted measurements using a similarly fabricated straight waveguide incorporated into a fiber-optic MZI. In this experiment, the output from the laser was split using a 90:10 fused fiber coupler, with the 90% output directed through a straight porous waveguide, as shown in Fig. 4(b). The size of the sensing window was identical between the straight waveguide and the integrated MZI. The outputs were recombined in a second, 50:50 fused fiber coupler and connected to a photodiode. The fiber based measurements used single-mode (non polarization-maintaining) fiber, and therefore require a polarization controller and

#191714 - $15.00 USD Received 4 Jun 2013; revised 19 Jul 2013; accepted 2 Aug 2013; published 12 Aug 2013

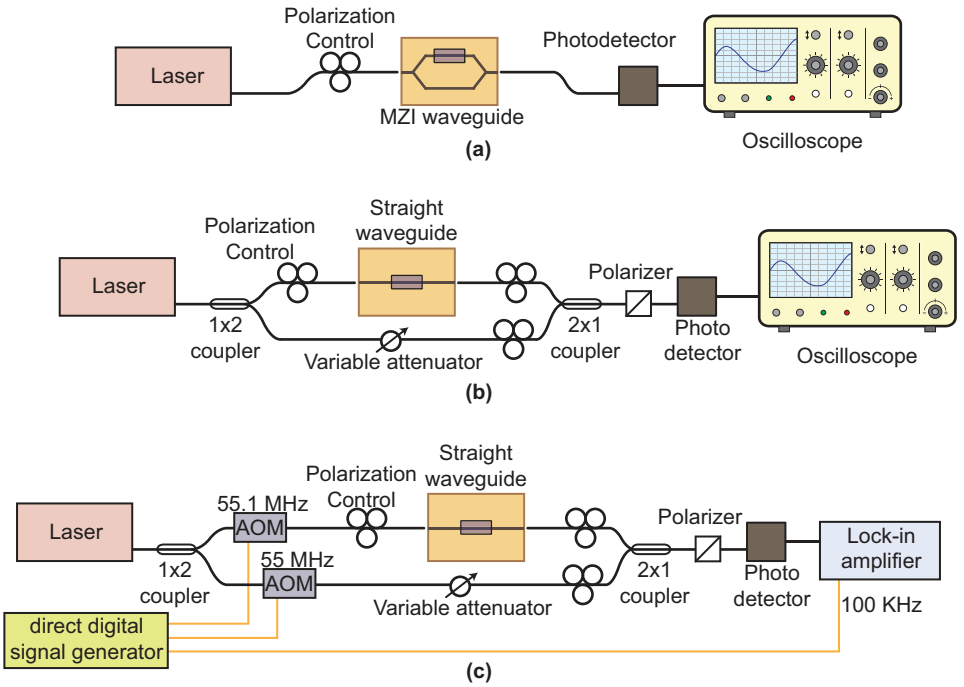

Fig. 4. Experimental setups used to conduct interferometric porous waveguide measurements. (a) Integrated Mach-Zehnder interferometer (MZI) constructed using porous silicon waveguides. (b) Fiber-based MZI, with porous waveguide incorporated in one arm of interferometer, and (c) Heterodyne fiber-based interferometer, enabling simultaneous measurement of magnitude and phase shift in porous waveguide sensor.

polarizer to ensure that the signals from the two arms of the interferometer remain co-polarized. By contrast, the integrated MZI shown in Fig. 4(a) maintains the polarization state in the two arms.

Finally, in order to clearly differentiate phase and amplitude changes, we also conducted optical heterodyne phase measurement with the same straight waveguide, using the system depicted in Fig. 4(c). Two acoustooptic modulators (AOM) were employed on both branches of fiber optic MZI, to shift frequency of sensing branch by 55.1 MHz and reference branch by 55.0 MHz. The magnitude of the resulting 100 kHz beat-signal was observed using a dual-phase lock-in amplifier with 100 kHz reference frequency. The relative phase and intensity of the optical signal is then translated into the magnitude and phase of the 100 kHz heterodyne signal.

Figure 5 compares the stability between the integrated MZI shown in Fig. 4(a) and the corresponding fiber-based interferometer of Fig. 4(b), measured over a 400 second interval, when there is no analyte introduced to the sensor. To ensure an accurate comparison between the measurements, the optical powers were adjusted prior to the observation to ensure that both devices show full fringe contrast and have the peak output interferometric signal. The output of the MZI is nearly constant, indicating that the relative phase and intensity in the interferometer remains stable over the observation time. The fiber-based interferometer shows a significant slow drift of the output signal, associated with uncontrolled mechanical and thermal instabilities in the fiber and waveguide. In comparison to the fiber-based interferometer, the integrated MZI uses shorter arms that are integrated on the same chip in close proximity. Because the

#191714 - $15.00 USD Received 4 Jun 2013; revised 19 Jul 2013; accepted 2 Aug 2013; published 12 Aug 2013

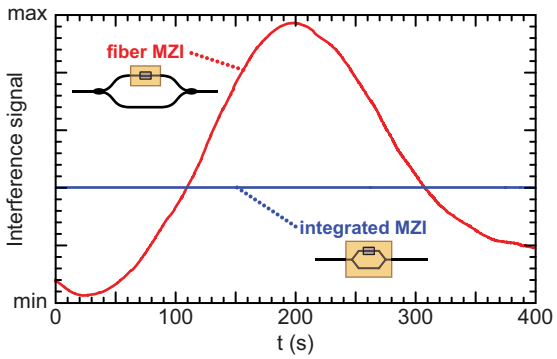

Fig. 5. Comparison of stability from integrated porous Mach-Zehnder interferometer and fiber-based waveguide interferometer, conducted over 400 s with no analyte present. Prior to observation, both systems were adjusted to have full interferometric fringe contrast and equal fringe amplitude.

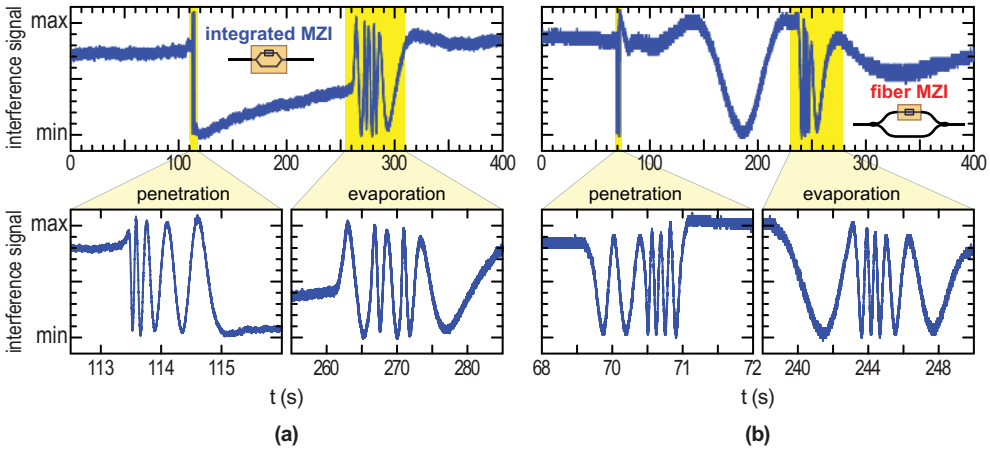

Fig. 6. Interference signal measured from (a) integrated nanoporous silicon MZI device and (b) straight waveguide incorporated into an external fiber MZI. The interference signal is observed over a 400 s time interval during which a drop of isopropanol is introduced to the porous waveguide.

#191714 - $15.00 USD Received 4 Jun 2013; revised 19 Jul 2013; accepted 2 Aug 2013; published 12 Aug 2013

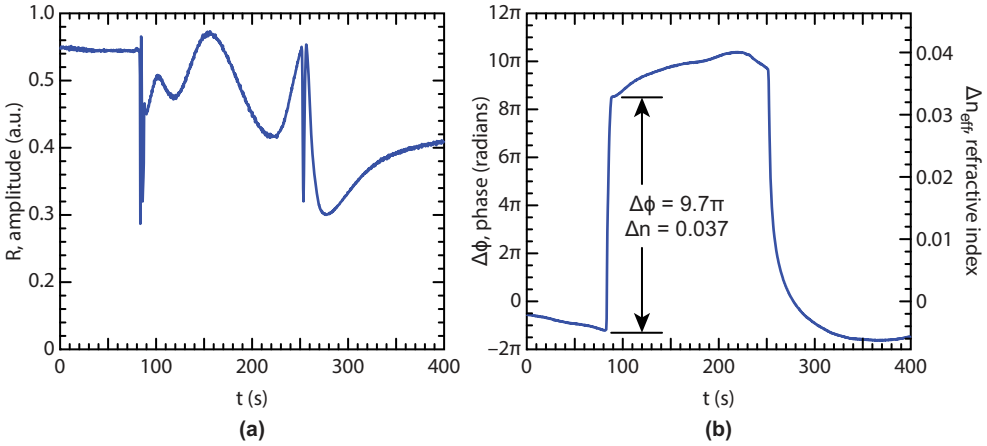

Fig. 7. Heterodyne measurement of intensity and phase change from a 200 μm porous silicon waveguide that is exposed to isopropanol.

measurement responds only to the relative phase difference between the arms, any thermal and mechanical fluctuations that are common to the two arms will cancel, leading to the stable response observed in Fig. 5.

To demonstrate the sensor performance, we applied a drop of isopropanol to the active region of the waveguide using a micro-pipette, while observing the detected signal on an oscilloscope. Figure 6(a) plots the received signal from the integrated MZI device, measured over a 400 second interval during which the isopropanol was introduced. The enlarged plots in the lower panel below show the rapid phase shift (approximately 5 fringes over 2 seconds) that occurs when the analyte immediately penetrates the porous waveguide. This process later reverses as the analyte evaporates out of the pores. A similar evolution is seen in the fiber-based interferometer, as shown in Fig. 6(b) but the response is superposed onto a slow, unrepeatable drift associated with thermal and mechanical instability of the fiber-based interferometer. The additional interference fringe in between penetration and evaporation seen in Fig. 6(b) is a consequence of the instability of the fiber-based interferometer, and does not reflect the true refractive index change caused by the analyte.

Figure 7 plots optical intensity and phase, measured using the fiber-based heterodyne system shown in Fig. 4(c). When the isopropanol penetrates the waveguide, we see a rapid increase in the phase by approximately 9.7π, which agrees well with the fringe measurement obtained from the MZI. Upon evaporation, the phase shows a slower recovery to its original level.

To estimate the sensitivity of the interferometric measurement, we relate the measured phase shift $\Delta\phi$ to the effective refractive index shift Δn_{eff} through the following relation:

$$\Delta n_{\text{eff}} = \frac{\Delta\phi\lambda}{2\pi L} \tag{1}$$

where λ is vacuum wavelength (1.55μm) and L is interaction length (200 μm). The right axis in Fig. 6(b) shows the calculated refractive index shift of the waveguide, which shows a reversible refractive index shift of 0.04 refractive index units (RIU) caused by the isopropanol. From Eq. 1, we estimate the sensitivity of 13,000 rad/RIU·cm. Assuming that the integrated MZI device has a limit of detection of 0.1 radian (5.7 degrees), a conservative estimate based on the data presented in Figs. 5 and 6, the device should be capable of detecting a refractive index change as small as 10^{-5} if the active area were increased to L = 1 cm.

#191714 - $15.00 USD Received 4 Jun 2013; revised 19 Jul 2013; accepted 2 Aug 2013; published 12 Aug 2013

Although the test analyte considered imparts a relatively large phase shift, the sensitivity estimated here is predicated on the assumption that the induced phase shift will be strictly proportional to the refractive index, as expressed in Eq. 1, even for smaller changes in the refractive index.

For comparison, the highest sensitivity porous silicon based optical sensors reported to date have used spectral measurements of resonant cavities [14]. These methods report a spectral sensitivity of 300-500 nm/RIU (meaning, for example, that with a spectral resolution of 0.1 nm, a refractive index shift as small as 2×10^{-4} could be detected.) By using prism or grating-based coupling into slab waveguides (with no transverse confinement), a sensitivity as high as 1000 nm/RIU has been reported [22, 29]. The integrated MZI reported here has the potential to exceed the sensitivity of existing approaches, in a simple device that is both stable and compact.

It should be acknowledged that the laser-based heterodyne interference measurement reported here, while more capable, is a more costly and sophisticated measurement than broadband reflectance spectrometry previously employed in planar porous silicon sensors [7–15]. However, the integrated MZI device could be easily modified by introducing an intentional path length difference between the arms, which would enable observation of interference fringes in transmission using broadband optical spectroscopy.

4. Conclusion

We describe the fabrication and measurement of an integrated nanoporous Mach-Zehnder interferometric waveguide sensor. Nanoporous silicon single mode integrated waveguides were successfully fabricated by electrochemical etching and direct-write laser oxidation. The nanoporous dielectric permits direct infiltration of the analyte gas or liquid into the waveguide core, enabling sensitive detection in a small device – thereby overcoming a key disadvantage of evanescent-mode sensors. Using isopropanol as a test analyte, we observed a phase shift of 9.7π in an interaction length as short as 200 μm. Sensitivity of 13000 rad/RIU-cm was measured which exceed most previous reports.

Acknowledgment

This work was partially supported by NSF CBET award 0932673. The microscopy and device fabrication was carried out with at the University of Maryland Nanocenter.

#191714 - $15.00 USD Received 4 Jun 2013; revised 19 Jul 2013; accepted 2 Aug 2013; published 12 Aug 2013